ACS Catalysis

Letter

pubs.acs.org/acscatalysis

Supported Single Pt_1/Au_1 Atoms for Methanol Steam Reforming

Xiang-Kui Gu,[†,‡] Botao Qiao,[§,†,‡] Chuan-Qi Huang,[†] Wu-Chen Ding,[†] Keju Sun,[†] Ensheng Zhan,[§,†] Tao Zhang,[†] Jingyue Liu,*[,§,†] and Wei-Xue Li*[,†]

[†]State Key Laboratory of Catalysis, Dalian Institute of Chemical Physics, Dalian National Laboratory for Clean Energy, Chinese Academic of Sciences, Dalian 116023, China

[§]Department of of Physics, Arizona State University, Tempe, Arizona 85287, United States

Supporting Information

ABSTRACT: The single Pt_1 and Au_1 atoms stabilized by lattice oxygen on ZnO{10$\bar{1}$0} surface for methanol steam reforming is reported. Density functional theory calculations reveal that the catalysis of the single precious metal atoms together with coordinated lattice oxygen stems from its stronger binding toward the intermediates, lowering reaction barriers, changing on the reaction pathway, enhancing greatly the activity. The measured turnover frequency of single Pt_1 sites was more than 1000 times higher than the pristine ZnO. The results provide valuable insights for the catalysis of the atomically dispersed precious metals on oxide supports.

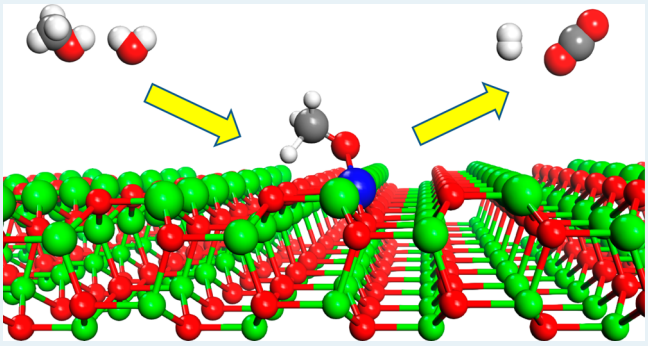

KEYWORDS: *single atom catalysis, methanol steam reforming, density functional theory, electron microscopy, activity, selectivity*

In heterogeneous catalysis, metal particles are used to catalyze various industrially important chemical processes. To effectively utilize the desired, often expensive, precious metal, one usually disperses them onto high-surface-area supports with sizes ranging from a few nanometers down to subnanometers.[1−4] The presence of a large number of low-coordination sites on small particles is thought to be responsible for the enhanced catalytic activity.[5] To fully understand the structure−reactivity relationship of small particles or clusters, however, requires detailed knowledge of the active sites at the atomic level, which are often not available. Alternatively, metal species atomically dispersed onto oxide supports provide a well-defined system and have demonstrated excellent catalytic performance.[6] Moreover, such systems can provide a new platform to mimic homogeneous catalysis under heterogeneous environment.[7,8] Due to the recent advances of atomic resolution and in situ characterization techniques,[9] there is increasing interest in studying atomically dispersed catalysts. Furthermore, it is found that the active centers, responsible for the low-temperature activity of the water-gas-shift reaction[10,11] and CO oxidation,[12,13] can be attributed to the function of individual precious atoms strongly anchored onto the surfaces of oxide supports. Although the atomically dispersed catalysts may open a new and probably an efficient way to design novel classes of heterogeneous catalysts, it remains a challenge to fully uncover the nature of the active sites, to significantly improve their performance, and to develop strategies to prolong the stability of single-atom catalysts.

To address these questions, we report here a density functional theory (DFT) calculation, subangstrom resolution scanning transmission electron microscopy (STEM) characterization, and catalytic reactivity studies of single Pt_1 and Au_1 atoms dispersed onto ZnO nanowires (NWs) for methanol steam reforming (MSR).[14−16] The single Pt_1 and Au_1 atoms with atomic dispersion on ZnO was successfully prepared and identified to locate at the surface Zn lattice sites and stabilized by the lattice oxygen. Theoretical calculations show unambiguously that the single precious metal atoms together with coordinated oxygen bind more strongly toward the intermediates, improve the reaction energetics and kinetics, and change the reaction pathway. These eventually lead the single Pt_1 sites as the active sites with 1000 times higher turnover frequency (TOF) for MSR than that of the pristine ZnO.

ZnO NWs used in this work consist primarily of {10$\bar{1}$0} facets (Figure S1a), and a loading of 0.0125 wt % of Au or Pt on ZnO NWs were prepared, as detailed in Supporting Information. Representative high-angle annular dark-field (HAADF) images of the Pt_1/ZnO and Au_1/ZnO catalysts are shown in Figure 1a,b, where the ZnO NWs were tilted with the electron beam close to [10$\bar{1}$0] and [11$\bar{2}$0] zone axis of ZnO (Figure S1b), respectively. The brighter dots represent single Pt and Au atoms (indicated by the yellow arrow) located on the Zn columns of the ZnO NW (denoted as Pt_1 and Au_1 hereafter). These isolated single atoms were relatively stable under electron beam irradiation, suggesting that they were anchored onto ZnO{10$\bar{1}$0}. After analyses of many low- and high-magnification HAADF images (Figure S1c and d), we

Received: May 30, 2014
Revised: August 17, 2014

   dx.doi.org/10.1021/cs500740u | ACS Catal. 2014, 4, 3886−3890

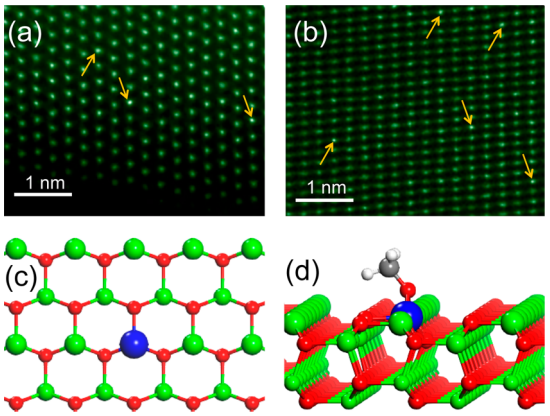

Figure 1. HAADF-STEM images of ZnO{10$\bar{1}$0} nanowires with embedded Pt_1 (a) and Au_1 (b) atoms (indicated by the yellow arrow), respectively. (c) Schematic structure for $Pt_1/Au_1/ZnO\{10\bar{1}0\}$ (top view) and (d) $Pt_1/Au_1/ZnO\{10\bar{1}0\}$ with adsorbed CH_3O^* (side view). The blue, green, red, gray, and white spheres represent Pt_1/Au_1, Zn, O, C, and H atoms, respectively.

concluded that there were no Pt or Au clusters/particles in these $Pt_1/Au_1/ZnO$ catalysts.

The stability of $Pt_1/Au_1/ZnO$ can be explained if the observed single Pt_1 or Au_1 atoms are assumed to anchor onto the corresponding {10$\bar{1}$0} surface Zn vacancy positions (Figure 1c,d). DFT calculations showed that the corresponding formation energies of single Pt_1 and Au_1 atom are 0.22 and 0.86 eV lower than the reservoirs in equilibrium with infinite large metal counterparts, implying that the embedded Pt_1 and Au_1 are thermodynamically stable and resistant to segregation or agglomeration during the synthesis and/or the catalytic reactions. Pt_1 or Au_1 substituted at the subsurface Zn lattice sites would raise the corresponding energies by 0.45 and 0.70 eV and is energetically less favorable. On the other hand, the Pt_1 or Au_1 atoms positioned on top of the surface Zn sites is unstable and would displace to the bridge sites between Zn and O atoms at the grooves of ZnO{10$\bar{1}$0}, which was not observed. The stability of the Pt_1/Au_1 sites originates from the strong chemical bonding between Pt_1/Au_1 and the coordinated lattice oxygen, as seen from the extensive charge redistribution in Figure S2. Accordingly, Pt_1/Au_1 atoms are in the cationic state.

The presence of surface embedded Pt_1/Au_1 atoms changes dramatically the adsorption sites, their binding strength, and reaction energetics and barriers on the ZnO{10$\bar{1}$0} surface. The calculated binding energies for the reactants and intermediates involved in MSR at the most favorable site (Table S1 and Figure S3) are given in Figure 2. For CH_3O^*, HCHO*, HCO*, CO*, and OH*, the corresponding binding strengths increase considerably by at least 0.99 eV on Pt_1/ZnO, whereas at least 0.46 eV (maximum 1.84 eV) on Au_1/ZnO. For H_2O^* and CH_3OH^*, the binding strengths increase only slightly, less than 0.15 eV in maximum on both Pt_1/ZnO and Au_1/ZnO. The presence of Pt_1 and Au_1 atoms also decrease the formation energies of the oxygen vacancy by at least 1.31 eV. This result agrees well with the previous calculations,[17] where the different valence of the substituted metal atoms from the host plays an essential role. These trends of variation in the binding energy are consistent with previous calculations.[18] The enhanced binding of the reactants/intermediates and decreased vacancy formation energy of oxygen due to the presence of Pt_1/Au_1

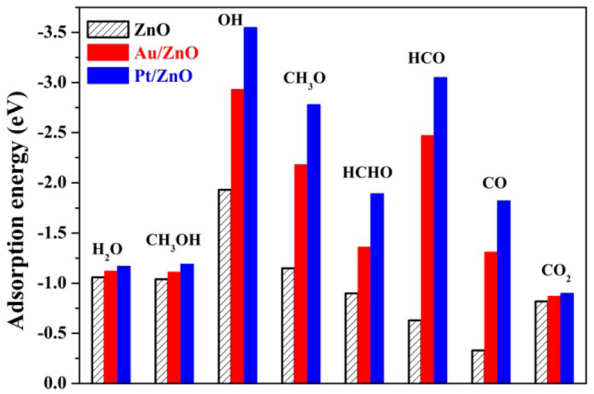

Figure 2. Calculated binding energies of the reactants and intermediates involved in MSR on ZnO{10$\bar{1}$0}(shadow), Au_1 (red solid), and Pt_1 (blue solid) embedded ZnO{10$\bar{1}$0}.

atoms improve reaction energetics and the subsequent reactivity, as detailed in below.

The significantly enhanced bonding of the reaction intermediates originates from their direct coordination to the Au_1/Pt_1 atoms, as seen, for instance, from the CH_3O^* adsorption structure in Figure 1d (additional detail in Figure S3). To reveal the electronic origin, the projected density of states (PDOS) is plotted in Figure S4. Compared to the Zn PDOS, there are considerable states available around the Fermi level for Pt_1 and Au_1, which would make them more active. Moreover, the larger spatial extension of Pt_1 and Au_1 d-orbitals than that of Zn allows more extensive charge transfer and redistribution, as seen clearly from the charge density difference (Figure S5), forming a stronger chemical bond with the intermediates, accordingly.

The influence of the Pt_1/Au_1 atoms on the dehydrogenation of H_2O^* and CH_3OH^* toward OH*, CH_3O^*, and CH_2O^* (the initial elementary reaction steps in MSR) were calculated and plotted in Figure 3a (tabulated in Table S2). In terms of energetics, the sum of the binding energies of two reactants (H_2O^* and CH_3OH^*) on Pt_1/ZnO is 0.26 eV lower than those on ZnO. Moreover, the reaction energetics ΔE for the O−H bond scission of H_2O^* and CH_3OH^* are exothermic (−0.27

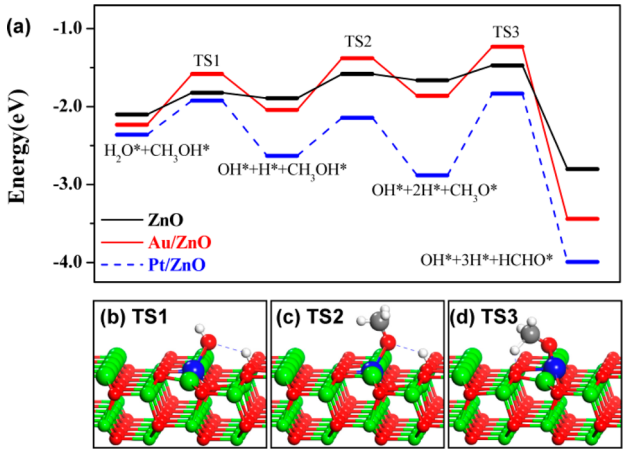

Figure 3. (a) Calculated potential energy surfaces for CH_3OH^* + H_2O^* → CH_2O^* + OH* + 2H* on ZnO, Au_1/ZnO, and Pt_1/ZnO. (b), (c), and (d) are the schematic structures for the transition state TS1, TS2, and TS3 on $Pt_1/Au_1/ZnO\{10\bar{1}0\}$, respectively. The energy reference is gas phase H_2O and CH_3OH.

dx.doi.org/10.1021/cs500740u | ACS Catal. 2014, 4, 3886−3890

and −0.25 eV) on Pt_1/ZnO, respectively, in contrast to the endothermic (0.21 and 0.23 eV) on ZnO. For the subsequent C−H bond scission of CH_3O* to HCHO*, the difference of ΔE between Pt_1/ZnO and ZnO is however negligible. The stronger binding of the reactants and favorable reaction energetics on Pt_1/ZnO than those on ZnO improve the overall energetics and therefore the corresponding reactivity. This has also been found for water dissociation on Pd-doped ZnO.[19] On the other hand, the calculated reaction barriers E_a for the above three reaction steps are 0.44, 0.49, and 1.05 eV with the corresponding transition states TS1, TS2, and TS3 in Figure 3b, 3c, and 3d, respectively, which are all higher than those on ZnO (0.28, 0.31, and 0.19 eV). Such a behavior suggests that the overall potential energy surface (PES) becomes corrugated. Nevertheless, as seen from Figure 3a, the downshift of PES on Pt_1/ZnO, a consequence of the stronger binding of the reactants and improved ΔE for the O−H bond scissions, is so significant that the corresponding TSs (blue bar) remains energetically lower than those of TSs (black bar) of ZnO. This implies that Pt_1/ZnO would have a higher reactivity than ZnO.

For Au_1/ZnO, the overall binding of two reactants enhances modestly by ∼0.14 eV compared to ZnO. Reaction energetics ΔE in the subsequent O−H scissions remains endothermic (0.19 and 0.18 eV), similar to those of ZnO. However, the corresponding O−H scission barriers E_a (0.65 eV for H_2O* and 0.66 eV for CH_3OH*) become even larger than those on Pt_1/ZnO (0.44 and 0.49 eV). Namely, the Au_1/ZnO does not possess appreciable improvement in binding the reactants or the reaction energetics than those of ZnO, whereas the corresponding overall PES becomes more corrugated than that of ZnO. As a result, the values of the TSs (red bar in Figure 3a) are energetically even higher than those of ZnO (black bar).

The MSR experiments were carried out in a fixed-bed reactor with 50 mg of catalyst in about 60−80 mesh size. Pristine ZnO, Pt_1/ZnO, and Au_1/ZnO NWs were tested. The products were H_2, CO, and CO_2 only within the detection limit, and the conversion was calculated based on the carbon balance. All three catalysts were very stable during the MSR reaction at 390 °C (Figure 4a). On the pristine ZnO NWs, the conversion was low (<10%), but the selectivity toward CO_2 approached 100%, which agrees well with the recent literature reports.[20,21] The Pt_1/ZnO catalyst was much more active than that of the pristine ZnO with the corresponding conversion of about 43% at the steady state. The selectivity toward CO_2 remained high, ca. 88%. The Au_1/ZnO catalyst was also much more active than the pristine ZnO NWs with a conversion of about 28% and nearly 100% CO_2 selectivity.

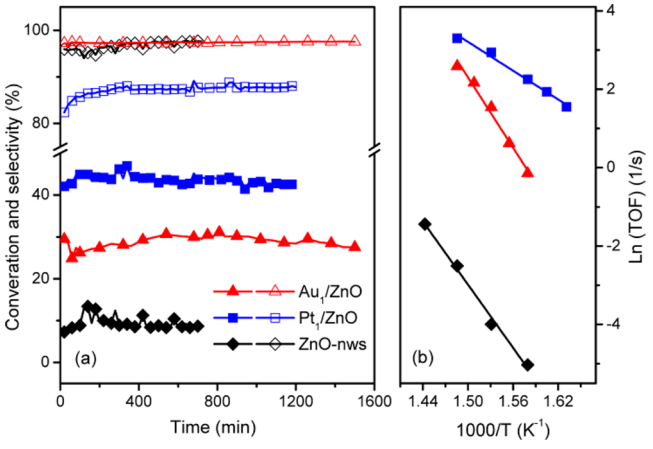

Figure 4. (a) Methanol conversion (solid) and CO_2 selectivity (open) as a function of reaction time at 390 °C on Au_1/ZnO (red triangle), Pt_1/ZnO (blue square) catalysts, and the pristine ZnO nanowires (black diamond); (b) corresponding Arrhenius plots of the reaction rate Ln (TOF) (s^{-1}) versus $1/T$ for the MSR reaction.

Taking into account the extremely low levels of Pt and Au loading (only about 125 ppm), the differences in TOF values between these single-atom catalysts and the pristine surfaces of ZnO (measured in a kinetically controlled regime with methanol conversion less than 20%) will be huge. For the pristine ZnO NWs primarily exposing $\{10\bar{1}0\}$ surfaces with a total surface area of ∼10 m^2/g, the corresponding TOF for MSR was calculated by assuming that all the Zn sites in the topmost layer of the ZnO surface are active centers. The calculated TOF at 380 °C is 1.8×10^{-2} s^{-1}. For the Pt_1/ZnO and Au_1/ZnO catalysts, after subtracting the contribution from the surface Zn sites of the ZnO NWs, the corresponding TOF solely from the embedded Au_1 and Pt_1 sites for MSR were estimated to be 4.7 and 18.9 s^{-1}, respectively, about two and three orders of magnitude higher than that of ZnO.

The TOF at different T varying from 340 to 420 °C were measured. The corresponding Arrhenius plots are shown in Figure 4b, from which the apparent activation energies E_{app} and pre-exponential factors A_{app} can be extracted. The E_{app}, from lower to higher values, are 1.05, 2.32, and 2.58 eV for Pt_1/ZnO, ZnO, Au_1/ZnO, respectively, with the corresponding A_{app} of 2.4×10^9, 1.7×10^{16}, 3.2×10^{20} s^{-1}. The remarkable different A_{app} could be rationalized by the so-called compensation effect with respect to the corresponding E_{app} of the Arrhenius law found from various activation processes.[22] Namely, when the apparent activation energy changes, so does the pre-exponential factor. Among three catalysts studied here, Pt_1/ZnO has the lowest E_{app} and the smallest A_{app}, whereas Au_1/ZnO has the highest E_{app} and the largest A_{app}. It is likely that the much lower E_{app} of the Pt_1/ZnO and higher A_{app} of the Au_1/ZnO explains their three and two orders of magnitude higher TOF than that of ZnO. We note that the MSR on ZnO powder catalysts has been studied and the measured E_{app} was found to be less than 100−200 kJ/mol.[20,21] The smaller E_a may have originated from the contribution of surfaces other than the $\{10\bar{1}0\}$ surfaces, for example, polar surfaces, or defect sites present in ZnO powder catalysts.

To rationalize further the experimental findings on the trend variation of the MSR activity and selectivity toward CO_2 and gain more mechanistic insights, the complete PESs on ZnO, Au_1/ZnO, and Pt_1/ZnO were explored thoroughly, and the most favorable reaction pathways are shown in Figure 5 (detailed energetics, barriers, and TSs in Table S2). The reaction pathway toward CO_2 could be classified into two pathways: Path I, association of formaldehyde from methanol with hydroxyl from water, and Path II, decomposition of formaldehyde to CO followed by water gas shift (WGS) reaction.[23] The pathway via methyl formate was not considered here because it was found to be of minor importance.[24]

First of all, we note that among all of the optimized TSs, only the order of the relative height of TS3 and TS4 in the optimized PES (Pt_1/ZnO < ZnO < Au_1/ZnO) follows the same order of the measured apparent activation energies. This indicates that either TS3 or TS4 could be the potential rate-determining state contributing to the measured apparent activation energy. Compared to TS4, the relative height of TS3 is higher, and would be more demanding to approach.

dx.doi.org/10.1021/cs500740u | ACS Catal. 2014, 4, 3886−3890

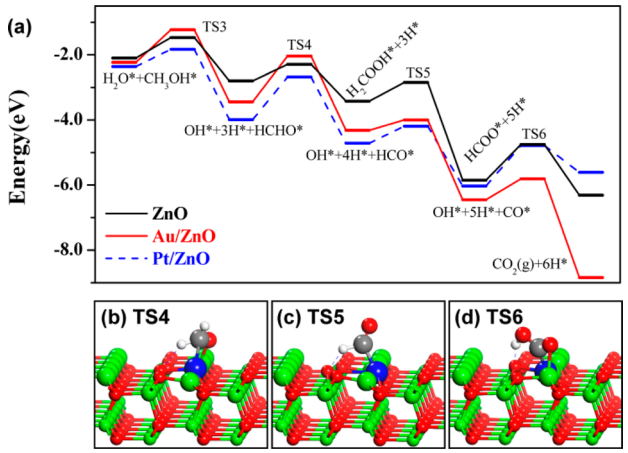

Figure 5. (a) Calculated most favorable reaction pathways for $CH_3OH^* + H_2O^* \rightarrow CO_2 + 6H^*$ on ZnO, Au_1/ZnO, and Pt_1/ZnO without showing TS1 and TS2 explicitly. (b), (c) and (d) are the schematic structures for the transition state TS4, TS5, and TS6 on $Pt_1/Au_1/ZnO\{10\bar{1}0\}$, respectively. The energy reference is gas phase H_2O and CH_3OH.

Actually, TS3 represents the highest TS in the optimized PES, irrespective to the three catalysts studied. In the literature, the energetically highest transition state in the PES of a multistep reaction was suggested to be the rate-determining state closely related to the apparent activation energy.[25] Accordingly, we attribute attentively TS3 (the dehydrogenation of methoxy to formaldehyde) as the rate-determining step of MSR for the three catalysts considered here.

For CO_2 selectivity on ZnO, the association of CH_2O^* with OH* to form H_2COOH^* (Path I) has a modest reaction barrier E_a of 0.51 eV and exothermic reaction energetics of −0.62 eV (TS4 in Figure S6). While for Path II, the dehydrogenation from CH_2O^* to CHO* has a considerably high barrier E_a of 1.51 eV and endothermic reaction energetics ΔE of 0.29 eV. Therefore, Path I is not only kinetically but also energetically more favorable than Path II. Once H_2COOH^* is formed, sequential dehydrogenation to HCOO* and CO_2 are exothermic with E_a of 0.57 and 1.10 eV (TS5 and TS6 in Figure S6), respectively. These results indicate that ZnO have a higher MSR selectivity toward CO_2, as evidenced by experiments.

On Pt_1/ZnO and Au_1/ZnO, because the overall binding energy of formaldehyde and hydroxyl is at least 1.46 eV stronger than those on ZnO, their association (Path I) becomes energetically less favorable, as seen from the change of reaction energetics from exothermic (−0.62 eV for ZnO) to endothermic (larger than 0.65 eV). Kinetically, it also becomes less favorable because the corresponding barrier increases at least by 0.49 eV. On the other hand, the binding of formyl (CHO*) on Pt_1/ZnO and Au_1/ZnO is at least 1.83 eV stronger than that on ZnO. Therefore, the reaction energetics for dehydrogenation of CH_2O^* to CHO* (Path II) would be improved. Indeed, the calculated reaction energetics changes from endothermic (0.29 eV for ZnO) to exothermic (−0.72 eV at least), concurrently with a decrease of barrier by 0.20 eV for Pt_1/ZnO and 0.11 eV for Au_1/ZnO (TS4, Figure 5b). The subsequent dehydrogenation of CHO* to CO* remains facile (TS5, Figure 5c). These considerations suggest that on Pt_1/ZnO and Au_1/ZnO complete dehydrogenation of formaldehyde rather than its association with hydroxyl becomes favorable. To evaluate the overall processes of Path II, the WGS reaction was studied. The calculated barriers of CO* association with OH* for CO_2 are 1.24 and 0.64 eV for Pt_1/ZnO and Au_1/ZnO, respectively (TS6, Figure 5d). The higher barrier for the previous one could be rationalized by the stronger binding of CO* by 0.52 eV at Pt_1 sites than Au_1 sites, hindering energetically the formation of CO_2. This final step would result in a lower CO_2 selectivity for Pt_1/ZnO than Au_1/ZnO, in agreement with experiment.

The calculations above show that although all the three catalysts have good selectivity toward CO_2, the corresponding reaction pathways are different when single atoms of Pt_1 or Au_1 are embedded onto the ZnO $\{10\bar{1}0\}$ surfaces. Therefore, the Pt_1 and Au_1 do not act as promoters; together with the oxygen and Zn sites of ZnO, they form new active centers that are intrinsically different from the catalytic properties of ZnO.

In summary, isolated precious metal atoms including Pt_1 and Au_1 together with coordinated lattice oxygen embedded onto ZnO surfaces provide single yet stable active sites for methanol steam reforming. Such single active sites bind stronger toward the intermediates, have a more favorable reaction energetics and kinetics, and even change the reaction pathways. These lead to a great enhancement of the activity, and in particular, the single Pt_1 sites embedded onto ZnO$\{10\bar{1}0\}$ surfaces were found to have a TOF of over 1000 times higher than that of the pristine ZnO. The results in this study for the function of the surface-embedded single precious metal atoms on supports provide valuable insights for the catalysis of the single precious metal atoms embedded on the oxide surfaces.

■ ASSOCIATED CONTENT

Ⓢ Supporting Information

Computational and experimental details, optimized reaction conditions and tests, calculated binding energies and reaction barriers, optimized structures and calculated charge density differences, and transition states for TS4, TS5, and TS6. This material is available free of charge via the Internet at http://pubs.acs.org.

■ AUTHOR INFORMATION

Corresponding Authors

*E-mail: jingyue.Liu@asu.edu.

*E-mail: wxli@dicp.ac.cn.

Author Contributions

‡X.-K.G. and B.Q. contributed equally.

Notes

The authors declare no competing financial interest.

■ ACKNOWLEDGMENTS

We are thankful for the financial support by the NSFC (nos. 21173210, 21103165, 21225315), 973 (no. 2013CB834603), and the start-up fund of the College of Liberal Arts and Sciences of Arizona State University (B.Q., E.Z., and J.L.). The authors also gratefully acknowledge the use of facilities in the John M. Cowley Center for High Resolution Electron Microscopy at Arizona State University, and calculations were carried out at the National Supercomputing Center "Tianhe-I" in Tianjin.

■ REFERENCES

(1) Turner, M.; Golovko, V. B.; Vaughan, O. P. H.; Abdulkin, P.; Berenguer-Murcia, A.; Tikhov, M. S.; Johnson, B. F. G.; Lambert, R. M. *Nature* **2008**, *454*, 981−984.

(2) Herzing, A. A.; Kiely, C. J.; Carley, A. F.; Landon, P.; Hutchings, G. J. *Science* **2008**, *321*, 1331−1335.
(3) Judai, K.; Abbet, S.; Worz, A. S.; Heiz, U.; Henry, C. R. *J. Am. Chem. Soc.* **2004**, *126*, 2732−2737.
(4) Lei, Y.; Mehmood, F.; Lee, S.; Greeley, J.; Lee, B.; Seifert, S.; Winans, R. E.; Elam, J. W.; Meyer, R. J.; Redfern, P. C.; Teschner, D.; Schlogl, R.; Pellin, M. J.; Curtiss, L. A.; Vajda, S. *Science* **2010**, *328*, 224−228.
(5) Remediakis, I. N.; Lopez, N.; Norskov, J. K. *Angew. Chem., Int. Ed.* **2005**, *44*, 1824−1826.
(6) Yang, X. F.; Wang, A. Q.; Qiao, B. T.; Li, J.; Liu, J. Y.; Zhang, T. *Acc. Chem. Res.* **2013**, *46*, 1740−1748.
(7) Liu, Z. P.; Wang, C. M.; Fan, K. N. *Angew. Chem., Int. Ed.* **2006**, *45*, 6865−6868.
(8) Motta, A.; Fragala, I. L.; Marks, T. J. *J. Am. Chem. Soc.* **2008**, *130*, 16533−16546.
(9) Liu, J. Y. *ChemCatChem* **2011**, *3*, 934−948.
(10) Zhai, Y. P.; Pierre, D.; Si, R.; Deng, W. L.; Ferrin, P.; Nilekar, A. U.; Peng, G. W.; Herron, J. A.; Bell, D. C.; Saltsburg, H.; Mavrikakis, M.; Flytzani-Stephanopoulos, M. *Science* **2010**, *329*, 1633−1636.
(11) Lin, J.; Wang, A.; Qiao, B.; Liu, X.; Yang, X.; Wang, X.; Liang, J.; Li, J.; Liu, J.; Zhang, T. *J. Am. Chem. Soc.* **2013**, *135*, 15314−15317.
(12) Qiao, B. T.; Wang, A. Q.; Yang, X. F.; Allard, L. F.; Jiang, Z.; Cui, Y. T.; Liu, J. Y.; Li, J.; Zhang, T. *Nat. Chem.* **2011**, *3*, 634−641.
(13) Lin, J.; Qiao, B. T.; Liu, J. Y.; Huang, Y. Q.; Wang, A. Q.; Li, L.; Zhang, W. S.; Allard, L. F.; Wang, X. D.; Zhang, T. *Angew. Chem., Int. Ed.* **2012**, *51*, 2920−2924.
(14) Palo, D. R.; Dagle, R. A.; Holladay, J. D. *Chem. Rev.* **2007**, *107*, 3992−4021.
(15) Zhang, C.; Yuan, Z.; Liu, N.; Wang, S. *Fuel Cells* **2006**, *6*, 466−471.
(16) Matsumura, Y.; Ishibe, H. *Appl. Catal., B* **2009**, *91*, 524−532.
(17) McFarland, E. W.; Metiu, H. *Chem. Rev.* **2013**, *113*, 4391−4427.
(18) Pala, R. G. S.; Metiu, H. *J. Catal.* **2008**, *254*, 325−331.
(19) Gu, X. K.; Ding, W. C.; Huang, C. Q.; Li, W. X. *Chin. J. Catal.* **2012**, *33*, 1427−1431.
(20) Lorenz, H.; Friedrich, M.; Armbruster, M.; Klotzer, B.; Penner, S. *J. Catal.* **2013**, *297*, 151−154.
(21) Halevi, B.; Lin, S.; Roy, A.; Zhang, H.; Jeroro, E.; Vohs, J.; Wang, Y.; Guo, H.; Datye, A. K. *J. Phys. Chem. C* **2013**, *117*, 6493−6503.
(22) Bligaard, T.; Honkala, K.; Logadottir, A.; Norskov, J. K.; Dahl, S.; Jacobsen, C. J. H. *J. Phys. Chem. B* **2003**, *107*, 9325−9331.
(23) Gu, X. K.; Li, W. X. *J. Phys. Chem. C* **2010**, *114*, 21539−21547.
(24) Lin, S.; Xie, D. Q.; Guo, H. *ACS Catal.* **2011**, *1*, 1263−1271.
(25) Kozuch, S.; Shaik, S. *Acc. Chem. Res.* **2011**, *44*, 101−110.